On the kinematic design of exoskeletons and their fixations with a human member

Nathanaël Jarrassé
Guillaume Morel

Univ. P. & M. Curie – Paris6, ISIR (Institut des Systèmes Intelligents et de Robotique) CNRS - UMR 7222
Emails : jarrasse@isir.fr, guillaume.morel@upmc.fr

***Abstract*— A crucial problem in developing robotic exoskeletons lies in the design of physical connexions between the device and the human limb it is connected to. Indeed, because in general the human limb kinematics and the exoskeleton kinematics differ, using an embedment at each connection point leads to hyperstaticity. Therefore, uncontrollable forces can appear at the interaction port. To cope with this problem, literature suggests to add passive mechanisms at the fixation points. However, empirical solutions proposed so far suffer from a lack of proper analysis and generality.**

In this paper, the general problem of connecting two similar kinematic chains through multiple passive mechanisms is studied. A constructive method that allows to determine all the possible repartitions of freed DoFs across the different fixation mechanisms is derived. It includes formal proofs of global isostaticity. Practical usefulness is illustrated through an example with conclusive experimental results.

I. Introduction

Exoskeletons are being designed for a growing number of applications, ranging from military applications [1] to rehabilitation [2]. For years, research in this field has followed a paradigm well summarized in [3]: *an exoskeleton is an external structural mechanism with joints and links corresponding to those of the human body* . In other words, designing the kinematics of an exoskeleton consists of replicating the human limb kinematics. This brings a number of advantages: similarity of the workspaces, singularity avoidance [4] and one-to-one mapping of human and robot joint force capabilities across the workspace.

The major drawback of this paradigm is that, in fact, human kinematics is impossible to precisely replicate with a robot. Indeed two problems occur:

1) morphology drastically varies between subjects
2) for a given subject, the joints kinematics are very complex and cannot be imitated by conventional robot joints [5].

In fact, it is impossible to find any consensual model of the human kinematics in the biomechanics literature due to complex geometry of bones interacting surfaces. For example, different models are used for the shoulder-scapula-clavicle group [6]. Discrepancies between the two kinematic chains thus seem unavoidable. Because of the connexions between multiple loops, this generates kinematic compatibility problems. Indeed, when connecting two-by-two the links of two kinematic chains that are not perfectly identical, hyperstaticity occurs. This phenomenon leads, if rigid models are considered, to the impossibility of moving and the appearance of non-controllable internal forces. In practice, though, rigidity is not infinite and mobility can be obtained thanks to deformations. When a robotic exoskeleton and a human limb are connected, most likely, these deformations occur at the interface between the two kinematic chains, due to the relatively low stiffness of human skin and tissues surrounding the bones [7].

Solutions found in the literature to cope with this problem are of three kinds. In a first approach, adaptation of the exoskeleton design to human limb kinematics is maximized. For example, robotic segments with adjustable length have been developed in [8]; a self alignment mechanism has been proposed in [9] ensuring that, at a given setup position, a 1 dof robot joint axis coincides with the human limb axis. These approaches may increase the kinematic compatibility between the robotic device and the human limb but perfect matching between the two chains does not seem to be achievable.

A second option consists of adding passive compliance at the fixations between the device and the limb. For example, pneumatic components have been used in [8] in order to introduce elasticity in the robot fixations and adaptability to variable limb section. This helps maintaining the hyperstatic forces low, but does not lead to canceling them, nor even to bound them to a known value.

The third approach consists in adding passive DoFs to connect the two kinematic chains, which is the most common way of eliminating hyperstaticty in multiloop mechanism design. This has been proposed back in the 1970s for passive orthoses, [10], [11]. The same principle has been recently used for a one degree of freedom device in [7], together with an *ad hoc* planar force transmission analysis. However, the literature proposes only empirical solutions and suffers from a lack of general and proven study of this crucial problem.

Rather, the constructive method proposed in this paper applies to a general spatial problem, which is properly formalized and solved thanks to a set of necessary and sufficient conditions for global isostaticity, see Section II. In Section III, the method is applied to ABLE, a given active 4DoF arm exoskeleton. In Section IV, experimental results illustrate the practical interest of the approach.

II. General methodology

The main question addressed in this paper is: given a proposed exoskeleton structure designed to approximately replicate a human limb kinematic model, how to connect it to the human limb while avoiding the appearance of uncontrollable forces at the interface? The answer takes the form of a set of passive frictionless mechanisms used to connect the robot and the subject's limb.

A. Problem formulation

The studied problem is depicted in Fig. 1. A human limb $\mathbf{H}$ and a robotic device $\mathbf{R}$ are connected through multiple mechanisms $\mathbf{L}_i$.

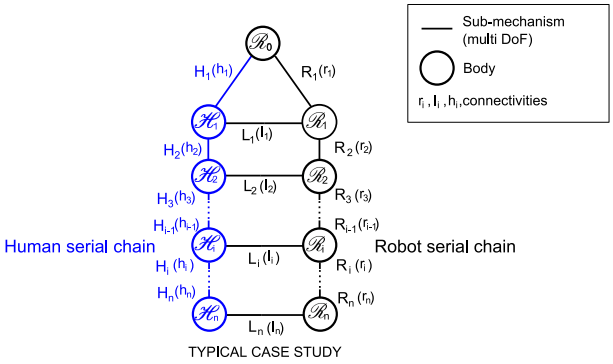

Fig. 1. Schematic of two serial chains parallel coupling

The base body of the exoskeleton is supposed to be attached to a body of the human subject. This common body is denoted $\mathscr{R}_0 \equiv \mathscr{H}_0$. The robot and the limbs are supposed to be connected through n fixations. Each fixation is a mechanism $\mathbf{L}_i$ for $i \in \{1,..,n\}$ consisting in a passive kinematic chain which connects a human body $\mathscr{H}_i$ to a robot body $\mathscr{R}_i$. Mechanisms $\mathbf{L}_i$ are supposed to possess a connectivity l_i. Recall that connectivity is the minimum and necessary number of joint scalar variables that determine the geometric configuration of the $\mathbf{L}_i$ chain [12]. Typically, $\mathbf{L}_i$ will be a nonsingular serial combination of l_i one DoF joints. The fixation can be an embedment ($l_i = 0$) or can release several DoFs, such that:

$$\forall i \in \{1,..,n\}, \quad 0 \leq l_i \leq 5 \quad . \tag{1}$$

Indeed choosing $l_i \geq 6$ would correspond to complete freedom between $\mathscr{H}_i$ and $\mathscr{R}_i$ which would not make any practical sense in the considered application.

Between $\mathscr{R}_{i-1}$ and $\mathscr{R}_i$, on the robot side, there is an active mechanism $\mathbf{R}_i$ which connectivity is denoted r_i. Similarly, between $\mathscr{H}_{i-1}$ and $\mathscr{H}_i$, on the human side, there is a mechanism $\mathbf{H}_i$ of connectivity h_i. Note that, due to the complexity of human kinematic h_i is not always exactly known, and literature from biomechanics provides controversial data on this point.

A proper design of mechanisms $\mathbf{L}_i$ with $i \in \{1,..,n\}$ shall guarantee that on one side, all the forces generated by the exoskeleton on the human limb are controllable and on the other side, there is no possible motion for the exoskeleton when the human limb is still. This is why in the next, the human limbs $\mathscr{H}_i$ are considered to be attached to the base body $\mathscr{R}_0$. This represents the case when the subject does not move at all. The resulting mechanism, depicted in Fig. 2, is denoted S_n.

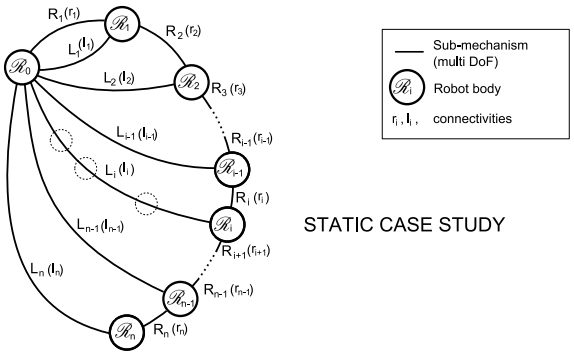

Fig. 2. Studied problem with a fixed human limb

Considering this overall mechanism, the two following properties shall be respected:

$$\forall i \in 1 \cdots n, \quad {}^{\mathbf{S}_n}T_i = \{0\} \quad \text{and} \tag{2a}$$

$$\forall i \in 1 \cdots n, \quad {}^{\mathbf{S}_n}W_{\mathbf{L}_i \to 0} = \{0\} \quad , \tag{2b}$$

where ${}^{\mathbf{S}_n}T_i$ is the space of twists describing the velocities of robot body $\mathscr{R}_i \in \mathbf{S}_n$ relative to $\mathscr{R}_0$ and ${}^{\mathbf{S}_n}W_{\mathbf{L}_i \to 0}$ is the space of wrenches (forces and moments) statically admissible transmitted through the $\mathbf{L}_i$ chain on the reference body $\mathscr{R}_0$, when the whole mechanism $\mathbf{S}_n$ is considered.

Equation (2a) expresses the fact that the mobility of any robot body connected to a human limb should be null when the human member is supposed to be still. Equation (2b) imposes that, considering the whole mechanism, there can be no forces of any kind exerted on the human limb. Indeed, since the actuators are supposed to apply null generalized forces, the presence of any force at the connection ports would be an uncontrollable force due to hyperstaticity. In the next, Eq. (2) is referred as the *global isostaticity condition*.

B. Conditions on the twist space dimensions

At first, denoting $\mathbf{S}_i$ the sub-mechanism constituted by the bodies $\mathscr{R}_0$ to $\mathscr{R}_i$, the chains $\mathbf{R}_0$ to $\mathbf{R}_i$ and $\mathbf{L}_0$ to $\mathbf{L}_i$, a recursive representation of $\mathbf{S}_i$ from $\mathbf{S}_{i-1}$ can be proposed, as illustrated in Fig. 3, where m_{i-1} is the connectivity of $\mathbf{S}_{i-1}$.

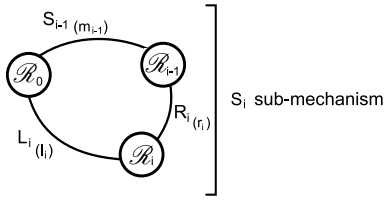

Fig. 3. Recursive structure of $\mathbf{S}_i$

In this convention, $\mathbf{S}_0$ represents a zero DoF mechanism while $\mathbf{S}_n$ is the whole studied mechanism. Thanks to the recursive nature of $\mathbf{S}_n$, and using the kinemato-static reciprocity

principle, it is possible to transform the global isostaticity condition into a set of equivalent conditions that concern the kinematic properties of each individual mechanisms $\mathbf{R}_i$ and $\mathbf{L}_i$, taken isolated. More precisely, the following proposition holds, as demonstrated in Appendix A.

Proposition 1: Conditions (2) are equivalent to :

$$\forall i \in 1 \cdots n, \quad dim(T_{\mathbf{S}_{i-1}} + T_{\mathbf{R}_i} + T_{\mathbf{L}_i}) = 6 \quad \textit{and} \tag{3a}$$

$$\forall i \in 1 \cdots n, \quad dim(T_{\mathbf{S}_{i-1}} \cap T_{\mathbf{R}_i}) = 0 \quad \textit{and} \tag{3b}$$

$$dim(T_{\mathbf{S}_n}) = 0 \quad , \tag{3c}$$

where $T_{\mathbf{S}_j} = {}^{\mathbf{S}_j}T_j$ is the space of twists describing the velocities of $\mathscr{R}_j$ relative to $\mathscr{R}_0$, when $\mathbf{S}_j$ is considered isolated from the rest of the mechanism (then it is different from ${}^{\mathbf{S}_n}T_j$), $T_{\mathbf{R}_i}$ is the space of twists produced by $\mathbf{R}_i$ – *i.e.* the space of twists of $\mathscr{R}_i$ relative to $\mathscr{R}_{i-1}$ if they were only connected through $\mathbf{R}_i$, $T_{\mathbf{L}_i}$ is the space of twists produced by $\mathbf{L}_i$ *i.e.* the space of twists of $\mathscr{R}_i$ relative to $\mathscr{R}_0$ if they were only connected through $\mathbf{L}_i$. ■

Remarkably, conditions (3) involve the space of twists generated by $\mathbf{R}_i$ and $\mathbf{L}_i$ when taken isolated, which is of great help for design purposes. In the next, these conditions are converted into constraints on the connectivities $r_i = dim(T_{\mathbf{R}_i})$ and $l_i = dim(T_{\mathbf{L}_i})$. To do so, it is supposed that kinematic singularities are avoided. In other words, summing the subspaces of twists will always lead to a subspace of maximum dimension given the dimensions of individual summed subspaces. This hypothesis will lead to determine how many DoFs shall be included in the passive fixation mechanisms $\mathbf{L}_i$. Of course as it is usual in mechanism design, when a particular design is finally proposed, it will be necessary to verify *a posteriori* the singularity avoidance condition.

C. Conditions on connectivities

The space of twists generated by $\mathbf{S}_i$ writes:

$$T_{\mathbf{S}_i} = T_{\mathbf{L}_i} \cap (T_{\mathbf{R}_i} + T_{\mathbf{S}_{i-1}}) \ . \tag{4}$$

This directly results from the space sum law that applies for serial kinematic chains and from the space intersection law that applies for parallel kinematic chains, see [13]. Furthermore, for any vector subspaces $\mathbf{A}$ and $\mathbf{B}$, $dim(\mathbf{A}) + dim(\mathbf{B}) = dim(\mathbf{A} + \mathbf{B}) + dim(\mathbf{A} \cap \mathbf{B})$. Therefore, denoting $m_i = dim(T_{\mathbf{S}_i})$, one has:

$$\begin{aligned} m_i &= dim(T_{\mathbf{L}_i}) + dim(T_{\mathbf{R}_i} + T_{\mathbf{S}_{i-1}}) - dim(T_{\mathbf{L}_i} + T_{\mathbf{R}_i} + T_{\mathbf{S}_{i-1}}) \\ &= dim(T_{\mathbf{L}_i}) + dim(T_{\mathbf{R}_i}) + dim(T_{\mathbf{S}_{i-1}}) - dim(T_{\mathbf{R}_i} \cap T_{\mathbf{S}_{i-1}}) \\ &\quad - dim(T_{\mathbf{L}_i} + T_{\mathbf{R}_i} + T_{\mathbf{S}_{i-1}}). \end{aligned}$$

If condition (3) is respected and under full rank asumption, one gets:

$$m_i = l_i + r_i + m_{i-1} - 6 \tag{5}$$

Finally, using $m_0 = 0$, this recursive equation simplifies to:

$$m_i = \sum_{j=1}^{i} (l_j + r_j) - 6.i \ . \tag{6}$$

For any vector subspaces $\mathbf{A}$, $\mathbf{B}$ and $\mathbf{C}$ of a vector space $\mathbf{E}$, $dim(\mathbf{A}+\mathbf{B}+\mathbf{C}) \leq dim(\mathbf{A}) + dim(\mathbf{B}) + dim(\mathbf{C})$; therefore, condition (3a) imposes that $\forall i \in 1 \cdots n, \quad m_{i-1} + r_i + l_i \geq 6$, or:

$$\forall i \in 1 \cdots n, \quad \sum_{j=1}^{i} (l_j + r_j) \geq 6.i \tag{7}$$

If $\mathbf{A}$ and $\mathbf{B}$ are two vector subspaces of $\mathbf{E}$ and $dim(\mathbf{A}) + dim(\mathbf{B}) > dim(\mathbf{E})$, then $\mathbf{A} \cap \mathbf{B} \neq \{0\}$, Eq. (3b) imposes that $\forall i \in 1 \cdots n, \quad m_{i-1} + r_i \leq 6$, or:

$$\forall i \in 1 \cdots n, \ \sum_{j=1}^{i-1} (l_j + r_j) + r_i \leq 6.i \tag{8}$$

Finally, from the last condition (3c), it is necessary that $m_n = 0$, or:

$$\sum_{j=1}^{n} (l_j + r_j) = 6.n \tag{9}$$

Thanks to these three last necessary conditions, it is now possible to calculate the different possible solutions for distributing the additional passive DoFs l_i along the structure:

- the possible choices for l_1 are such that $5 \geq l_1 \geq 6 - r_1$.
- for each choice of l_1, the possible choices for l_2 are such that $5 \geq l_2 \geq 12 - r_1 - r_2 - l_1$, etc.

This leads to a tree that groups all the admissible combinations for l_i, as illustrated in Fig 4.

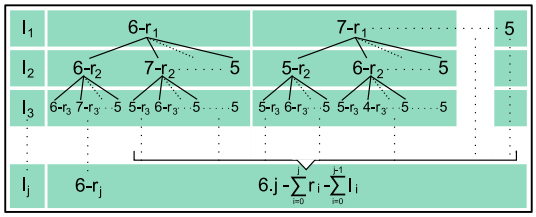

Fig. 4. Tree of possible solutions for the number of passive DoFs to add at every fixation point

Out of this tree, all the possible combinations of connectivities for the fixations are given. Of course, the selection among these solutions is to be made depending on the exoskeleton kinematics. Generally speaking, an important aspect to be considered is the force transmission: through any linear or rotational DoF that is not freed by the fixation mechanism, a force or a moment will be transmitted to the human limb, which is surrounded by soft tissues. Therefore, typically, transmitting moments would lead to locally deform the tissues which in turn can generate discomfort [14]. The next section illustrates, on a concrete spatial example involving two fixations, how to integrate this kind of considerations in the design of fixation mechanisms.

III. Application to a given exoskeleton

A. ABLE: an upper limb exoskeleton for rehabilitation

ABLE (see Fig. 5) is a 4 axis exoskeleton that has been designed by CEA-LIST [15] on the basis of an innovative screw-and-cable actuation technology, [16]. Its kinematics is

composed of a shoulder spherical joint involving $r_1 = 3$ coincident pivots and a 1 DoF pivot elbow ($r_2 = 1$). The forearm, terminated by a handle, is not actuated. Details on this robot can be found in [15].

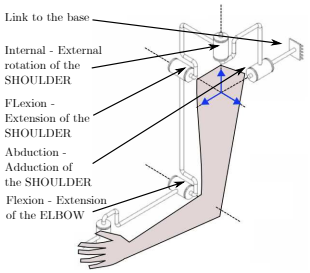

Fig. 5. Kinematics of ABLE

B. Fixations design for ABLE

In this section, the general method proposed in Sec. II is applied to ABLE, following three steps:

1) compute the tree of possible values for l_i;
2) choose among them a preferred solution by examining force transmission properties and kinematic complementarity;
3) verify a posteriori the full rank assumption, which is reported in Appendix B.

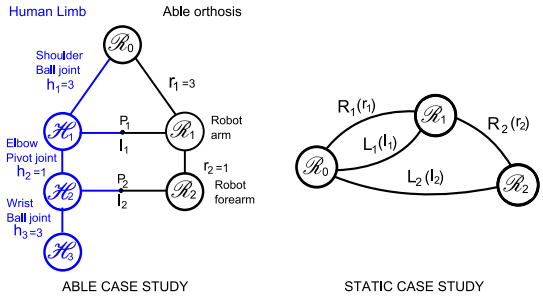

Fig. 6. Schematic of the ABLE and human arm coupling

Firstly, since ABLE comprises an upper arm and a forearm, two fixations shall be used (See Fig 6). The total number of passive DoF to be added is given by Eq. (9):

$$\sum_{j=1}^{n=2} l_j = 12 - \sum_{j=1}^{n=2} r_j = 12 - (3+1) \quad \Rightarrow l_1 + l_2 = 8 \qquad (10)$$

Moreover, for the first fixation, Eq. (7) and (8) give

$$6 - r_1 \leq l_1 \leq 6 \quad \Rightarrow \quad 3 \leq l_1 \leq 5\ . \qquad (11)$$

Since the total number of DoFs is fixed, the tree of possible solutions consists here of three parallel branches where l_1 is chosen between 3 and 5 and $l_2 = 8 - l_1$. Possible couples for (l_1, l_2) are (3,5), (4,4) and (5,3). Hereafter, these three options are analyzed in order to choose a preferred design among them.

- *Case a:* $l_1 = 3$ *and* $l_2 = 5$. In this case, both $\mathbf{S}_1$ taken isolated and $\mathbf{S}_2$ are isostatic, which corresponds to the most intuitive way of achieving global isostaticity. Degrees of freedom for $\mathbf{L}_1$ have to be chosen complementary to those of $\mathbf{R}_1$ in order to satisfy the full rank assumption. Since $\mathbf{R}_1$ is a ball joint that generates three independent rotational velocities around its center M_1, $\mathbf{L}_1$ must generate three independent linear velocities at point M_1. For example, three non coplanar translations could be used for $\mathbf{L}_1$. However, in this case, the fixation would transmit a null force, *i.e.* a pure couple around point P_1, which is defined as a point belonging to the humerus where fixation $\mathbf{L}_1$ is attached. This seems undesirable due to the torsion of the soft tissues that it would create around P_1 at the level of the attachment to the limb. Pure force transmission at point P_1 could be achieved by of using for $\mathbf{L}_1$ a ball joint centered at P_1. However, in this case, the full rank condition would not be respected because an internal motion corresponding to a rotation around $\vec{z}_1 = \frac{1}{\|\overrightarrow{M_1P_1}\|}\overrightarrow{M_1P_1}$ would occur. Finally, a preferred solution consists of choosing for $\mathbf{L}_1$ two pivot joints perpendicular to the upper arm main axis $\vec{z}_{arm}$ and one translation joint collinear to $\vec{z}_{arm}$. In this case, two forces perpendicular to $\vec{z}_{arm}$ and one moment around $\vec{z}_{arm}$ can be exchanged between the exoskeleton and the arm through $\mathbf{L}_1$. When designing $\mathbf{L}_2$, one shall further consider that, since $\mathbf{S}_1$ is isostatic, one has $m_1 = 0$. Therefore $\mathbf{L}_2$ is to be chosen kinematically complementary to $\mathbf{R}_2$, which is a pivot of axis $(M_2, \vec{z}_2)$. In other words, $\mathbf{L}_2$ must generate independently 2 rotations perpendicular to $\vec{z}_2$ and 3 velocities at point M_2. A natural solution is to choose a ball joint around P_2 and two translations in a plane perpendicular to $\vec{z}_2$. The resulting overall design is noted (a) and represented in Fig. 7.

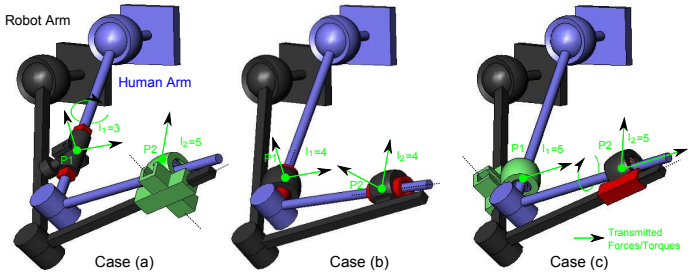

Fig. 7. Considered possibilities for coupling ABLE to an human arm. Case (a): Universal joint + 1 slide at P_1 and ball joint + 2 slides at P_2; case (b): Ball joint + 1 slide at both P_1 and P_2; case (c): Ball joint with 2 slides at P_1 and universal joint + 1 slide at P_2.

- *Case b:* $l_1 = 4$ *and* $l_2 = 4$. Note that in this case, $\mathbf{S}_1$ taken isolate is a 1 DoF mechanism, while only $\mathbf{S}_2$ is isostatic. Considering solution (a), 1 DoF must be added to $\mathbf{L}_1$ and 1 DoF must be removed from $\mathbf{L}_2$. Concerning $\mathbf{L}_1$, keeping freed the 3 DoF liberated for the isostatic solution (a), it seems preferable to choose, for the extra freed DoF, the rotation around z_1. Indeed, this will cancel the local tissue torsion due to moment transmission around $\vec{z}_1$. As a result, $\mathbf{S}_1$ is now a 1 DoF mechanism consisting of a pivot around $(M_1, \vec{z}_1)$. Concerning $\mathbf{L}_2$, the DoF to be removed from the solution (a) shall not degrade the dimension of $T_{\mathbf{S}_1} + T_{\mathbf{R}_2} + T_{\mathbf{L}_2}$. It seems preferable to keep the freed three rotations around P_2 and only

one translation along the forearm axis $\vec{z}_{forearm}$. Indeed, again, this choice avoids any torsion around P_2. Furthermore, it is shown in Appendix B that singular configurations of this solution, noted (b) and represented in Fig. 7 are easily identifiable and far away from nominal conditions of operation.

- *Case c:* $l_1 = 5$ *and* $l_2 = 3$. Similarly to solution (a), this combination will necessary lead to transmit at least one torsion moment around $\vec{z}_{forearm}$, as illustrated in Fig. 7 (solution (c)). Therefore, the finally preferred solution is (b).

Note that with solution (b), generating a moment to the human upper arm around $\vec{z}_{arm}$ is obtained by applying opposite pure forces perpendicular to $\vec{z}_{arm}$ at P_1 and to $\vec{z}_{forearm}$ at P_2 (see Fig. 8). Interestingly, this reproduces the method used

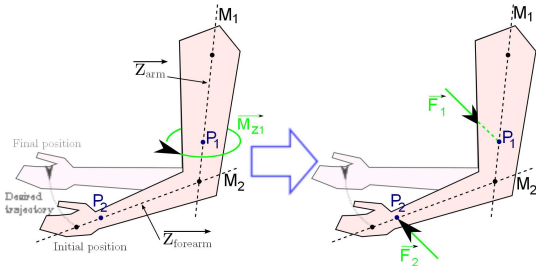

Fig. 8. Transmitting a moment around the upper arm axis with solution (a) (left) and (b) (right)

by physical therapists to assist patients in generating internal rotations of the shoulder without torsion to the tissue. As a price, the full extension configuration, when M_1, P_1 and P_2 are aligned, is singular, as detailed in the Appendix B. This configuration can be easily avoided by limiting the range of the elbow motion to a few degrees before full extension.

C. Fixations realization

The two fixations mechanisms are finally identical. They shall generate three independent rotations and one translation along the limb. The mechanism used to realize this function consists of three successive pivot joints which axis coincide and one slider whose axis is parrallel to human limb (see Fig. 9).

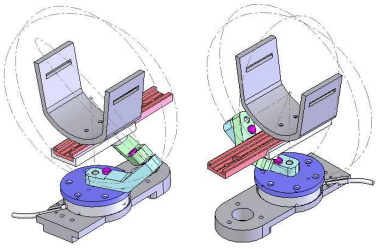

Fig. 9. Fixation simplification and realization (rear and front)

The fixations were dimensioned considering different constraints: $\mathbf{L}_2$ has to allow a wide range forearm pronosupination wile $\mathbf{L}_1$ shall not collide with arm tissues. As a result, possible motions left by the passive fixations have the ranges defined in Table I.

The fixations have been fabricated and mounted on ABLE. The upper arm fixation is placed near the elbow, just under

DoF	Arm Fixation	Forearm Fixation
Rotation1 ($\perp$ to the limb axis)	360 deg.	360 deg.
Rotation2 ($\perp$ to the limb axis)	90 deg.	90 deg.
Rotation3 (around the limb axis)	110 deg.	110 deg.
Translation	100mm	100mm

TABLE I

the triceps. The forearm fixation is placed near the wrist. Thermoformable material is used to form two splints adapted to human morphology. These splints are serially connected to the last fixation body. Note that the wrist splint blocks the wrist flexions, which are not studied here. Only pronosupination is allowed through $\mathbf{L}_2$ mobility.

Each fixation has been fitted with a force sensor placed on its base, on the robot side (ATI Nano43 6-axis Force/Torque sensor). This allows the reconstruction of the three forces and three moment components at P_1 and P_2.

For the experiments presented in the next section, in order to compare the forces involved with and without DoF liberation, the fixations have also been equipped with removable metallic pins, allowing to quickly lock the passive DoFs without detaching the subject from the exoskeleton.

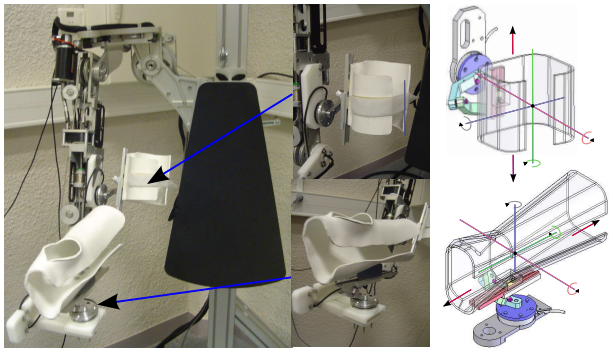

Fig. 10. The two fixations on the exoskeleton

IV. Experimental results

A. Experimental setup

An articulated mannequin was used for the experiments. Its arm possesses 5 passive DoFs (a ball joint shoulder, a pivot elbow and a pronosupination). Analyzing the interaction force and torque variations at the interfaces during the same movement with and without isostatic fixations allows to evaluate the impact on the appearance of uncontrolled forces.

The mannequin was placed in the exoskeleton and attached through the two fixations, see Fig. 11. During the experiments, the exoskeleton imposes a controlled trajectory, with a constant speed, to the mannequin arm. The experiment consists in a series of six simple point-to-point movements (with a limited range of motion) to the same target but reached with different joints postures, thanks to arm redundancy. Target is reached at constant and low speed (0.05 m/s) movement in order to limit inertial forces. Due to the high rigidity of the mannequin surface, and the large discrepancies between the robot and

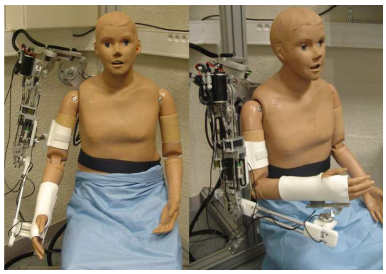

Fig. 11. Mannequin connected to the ABLE exoskeleton

mannequin kinematics, hyperstatism that occurs when fixation mechanisms are blocked generates large forces. Therefore, the movement range for each exoskeleton joint has been limited to 15 deg. in order not to destroy force sensors from overload.

The use of a mannequin controlled by exoskeleton allows to obtain a perfect repeatability during the experiments. This is really representative of co-manipulation cases where the robot generates a controlled motion by applying forces, as during robotic rehabilitation or movement assistance for impaired people.

B. Results and discussions

In Fig. 12, for each of the two F/T sensors, the absolute value of the measured force projected along the limb axis and norm of the measured moment, averaged during the experiments and across the six movements, are plotted. All

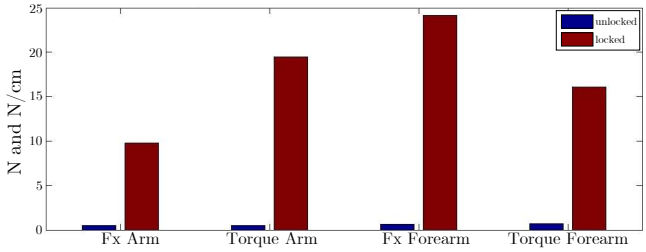

Fig. 12. Averaged absolute value of the undesired force $|F_x|$ and moments norm $\sqrt{(M_x^2+M_y^2+M_z^2)}$ on the two fixations (mean for the six movements)

these components result from hyperstaticity when fixations are locked and are theoretically fully canceled with passive mobile fixations $\mathbf{L}_1$ and $\mathbf{L}_2$. Figure 12 largely confirms the theoretical expectations. In Fig. 13, the norm of the components (F_y and F_z)corresponding to the components transmitted by the passive fixations is presented. The exoskeleton ability to transmit forces to the subject is not altered by the addition of $\mathbf{L}_1$ and $\mathbf{L}_2$.

V. Conclusion

In this paper a methodology aimed at designing the kinematics of fixations between an exoskeleton and a human member has been presented. Thanks to this method, isostatic fixations for a particular 4 DoF exoskeleton have been designed and their benefit on minimizing uncontrollable hyperstatic forces

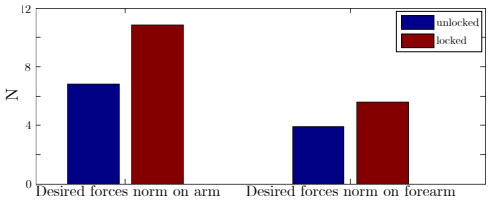

Fig. 13. Allowed forces ($\sqrt{(F_x^2+F_y^2)}$) norm on the two fixation (mean for the six movements)

at the human robot interface has been experimentally evidenced. These results show that the provided solution avoids hyperstaticity but also adapts to large variations of the human limb geometry without requiring a complex adaptable robot structure.

Future work will focus on explicit force control aspects, which is expected to be favored by the fact that only four components of forces have to be controlled from four joint motors.

Acknowledgments

This work was supported by the A.N.R. (Agence Nationale de la Recherche) with the projet BRAHMA (BioRobotics for Assisting Human Manipulation) PSIROB 2006.

Appendix

A. *Demonstration of Proposition 1*

1) Conditions (3) are sufficient: $[(3) \Rightarrow (2)]$.
We here suppose that conditions (3) are verified.
Because in $\mathbf{S}_n$, $\mathscr{R}_{i-1}$ is connected on one side to $\mathscr{R}_0$ through $\mathbf{S}_{i-1}$ and on the other side to $\mathscr{R}_i$ through $\mathbf{R}_i$ (see Fig. 3), one has:

$$\forall i \in \{1 \dots n\}, \quad {}^{\mathbf{S}_n}T_{i-1} = {}^{\mathbf{S}_{i-1}}T_{i-1} \cap \left[T_{\mathbf{R}_i} + {}^{\mathbf{S}_n}T_i\right] \quad , \qquad (12)$$

which is a recursive relationship for ${}^{\mathbf{S}_n}T_i$. Recalling that, by assumption, ${}^{\mathbf{S}_n}T_{\mathbf{S}_n} = \{0\}$ (condition 3c) and $T_{\mathbf{S}_{i-1}} \cap T_{\mathbf{R}_i} = \{0\}$ (condition 3b), this recursive law trivially leads to (2a).
Furthermore, the kinemato-static duality principle applied to the loop $(\mathscr{R}_0 \rightarrow \mathscr{R}_{i-1} \rightarrow \mathscr{R}_i \rightarrow \mathscr{R}_0)$ in Fig. 3 writes:

$$\forall i \in \{1 \dots n\}, \quad dim({}^{\mathbf{S}_i}W_{\mathbf{L}_i \rightarrow 0}) + dim(T_{\mathbf{S}_{i-1}} + T_{\mathbf{R}_i} + T_{\mathbf{L}_i}) = 6 \quad . \qquad (13)$$

Thanks to condition (3a), this leads to:

$$\forall i \in \{1 \dots n\}, \quad {}^{\mathbf{S}_i}W_{\mathbf{L}_i \rightarrow 0} = \{0\} \quad . \qquad (14)$$

Considering again the system $\mathbf{S}_i$ depicted in Fig. 3, and recalling that $\mathbf{L}_i$ and $\mathbf{R}_i$ are serial chains, one has, $\forall i \in \{1 \dots n\}$:

$${}^{\mathbf{S}_i}W_{\mathbf{L}_i \rightarrow 0} = {}^{\mathbf{S}_i}W_{\mathbf{L}_i \rightarrow i} = {}^{\mathbf{S}_i}W_{\mathbf{R}_i \rightarrow i} = {}^{\mathbf{S}_i}W_{\mathbf{R}_i \rightarrow i-1} = \{0\} \quad . \qquad (15)$$

Therefore, statically speaking, the multi-loop system $\mathbf{S}_{i-1}$ is in the same state when included in $\mathbf{S}_i$ than when isolated from the rest of the mechanism.

$$\forall i \in \{2 \dots n\}, \quad {}^{\mathbf{S}_i}W_{\mathbf{L}_{i-1} \rightarrow 0} = {}^{\mathbf{S}_{i-1}}W_{\mathbf{L}_{i-1} \rightarrow 0} \ ,$$

which, together with (14) recursively leads to condition (2b).

2) Conditions (3) are necessary : $\left[\overline{(3)} \Rightarrow \overline{(2)}\right]$.

Firstly, if condition (3c) is not verified, then ${}^{\mathbf{S}_n}T_n = T_{\mathbf{S}_n} \neq \{0\}$. In this case, (2a) is not satisfied.

Secondly, if (3b) is not verified, then $\exists i,\ (T_{\mathbf{R}_i} \cap T_{\mathbf{S}_{i-1}}) \neq \{0\}$. Thanks to Eq. (12), this leads to:

$$\exists i \in \{1 \cdots n\},\quad {}^{\mathbf{S}_n}T_{i-1} \neq \{0\} \quad , \tag{16}$$

which directly contradicts (2a).

Thirdly, if (3a) is not verified, i.e.:

$$\exists i,\ dim(T_{\mathbf{S}_{i-1}} + T_{\mathbf{R}_i} + T_{\mathbf{L}_i}) \leq 6 \quad , \tag{17}$$

then $\exists i,\ {}^{\mathbf{S}_i}W_{\mathbf{L}_{i\to 0}} \neq \{0\}$, meaning that $\mathbf{S}_i$ taken isolate is hyperstatic. Obviously, adding the rest of the mechanism to build $\mathbf{S}_n$, which consists of adding a parallel branch to $\mathbf{S}_i$ between $\mathscr{R}_0$ and $\mathscr{R}_i$ will not decrease the degree of hyperstaticity. Therefore $\exists i,\ {}^{\mathbf{S}_n}W_{\mathbf{L}_{i\to 0}} \neq \{0\}$, which contradicts condition (2b).

B. *Singularity analysis for ABLE and the two proposed fixation mechanisms*

The studied mechanism is depicted in Fig. 14: $\mathbf{R}_1$ is a ball joint which center is M_1; $\mathbf{L}_1$ is composed of a ball joint which center is P_1 (with $\overrightarrow{M_1P_1} = l_1.\overrightarrow{z_1}$ and $l_1 \neq 0$) and a slide along $(P_1, \overrightarrow{z_{arm}})$; $\mathbf{R}_2$ is a pivot joint which axis is $(M_2, \overrightarrow{x_2})$; $\mathbf{L}_2$ is composed of a ball joint which center is P_2 (with $\overrightarrow{M_2P_2} = l_2.\overrightarrow{z_2}$ and $l_2 \neq 0$) and a slide along $(P_2, \overrightarrow{z_{forearm}})$.

In order to find the singular configurations of this system, the necessary and sufficient conditions (3) are used.

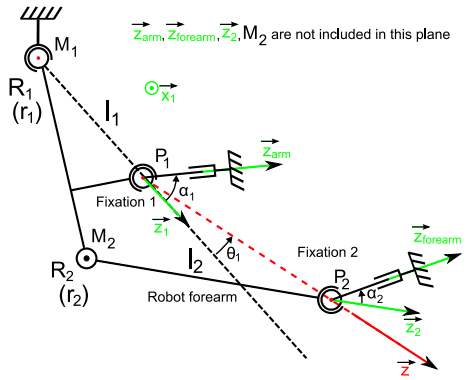

Fig. 14. Kinematics of ABLE + its fixations. The plane of the figure, perpendicular to $\vec{x}_1$, is defined by M_1, P_1 and P_2 while M_2 is off the plane.

1) Examination of Condition (3a)

- For $i = 1$, (3a) writes $dim(T_{\mathbf{R}_1} + T_{\mathbf{L}_1}) = 6$.

At point P_1, velocities allowed by $\mathbf{L}_1$ belong to the vector subspace $T_{\mathbf{L}_1} = span\{t_1, t_2, t_3, t_4\}$ and the velocities allowed by $\mathbf{R}_1$ belong to $T_{\mathbf{R}_1} = span\{t_5, t_6, t_3\}$, with

$$t_1 = (x_1^{\mathrm{T}}\ 0_3^{\mathrm{T}})^{\mathrm{T}},\quad t_3 = (z_1^{\mathrm{T}}\ 0_3^{\mathrm{T}})^{\mathrm{T}},\quad t_5 = (x_1^{\mathrm{T}}\ -l_1.y_1^{\mathrm{T}})^{\mathrm{T}}$$
$$t_2 = (y_1^{\mathrm{T}}\ 0_3^{\mathrm{T}})^{\mathrm{T}},\quad t_4 = (0_3^{\mathrm{T}}\ z_{arm}^{\mathrm{T}})^{\mathrm{T}},\quad t_6 = (y_1^{\mathrm{T}}\ l_1.x_1^{\mathrm{T}})^{\mathrm{T}}$$

Thus $T_{\mathbf{R}_1} + T_{\mathbf{L}_1} = span\{t_1, ..., t_6\}$. Defining

$$t'_5 = \frac{(t_6 - t_2)}{l_1} = (0_3^{\mathrm{T}}\ x_1^{\mathrm{T}})^{\mathrm{T}} \quad \text{and} \quad t'_6 = \frac{(t_1 - t_5)}{l_1} = (0_3^{\mathrm{T}}\ y_1^{\mathrm{T}})^{\mathrm{T}},$$

one can easily show that

$$\left[t_1\ t_2\ t_3\ t_4\ t'_5\ t'_6\right] = A\ \left[t_1\ t_2\ t_3\ t_4\ t_5\ t_6\right]$$

with $det(A) = \frac{1}{l_1^2}$. Since $l_1 \neq 0$, $\tau_1 = \{t_1, .., t_6\}$ is a basis of $\mathbb{R}^6$ if and only if $\tau_2 = \left\{t_1, .., t_4, t'_5, t'_6\right\}$ is a basis of $\mathbb{R}^6$. Consider now $a_i \in \mathbb{R},\ i \in \{1, .., 6\}$ such that:

$$a_1t_1 + a_2t_2 + a_3t_3 + a_4t_4 + a_5t'_5 + a_6t'_6 = 0 \tag{18}$$

It is trivial to show that $a_1 = a_2 = a_3 = 0$, $a_4d_z = 0$, $a_6 + a_4d_y = 0$ and $a_5 + a_4d_x = 0$ where $\overrightarrow{z_{arm}} = d_x\overrightarrow{x_1} + d_y\overrightarrow{y_1} + d_z\overrightarrow{z_1}$. If $d_z \neq 0$ then $a_6 = a_5 = a_4 = 0$ and τ_2, then τ_1 are bases of $\mathbb{R}^6$. On the contrary, if $d_z = 0$, there exists a non null combination of a_i that verifies (18) which means that τ_2 and τ_1 are not bases anymore. Condition (3a) is thus verified for $i = 1$ if and only if $d_z = \overrightarrow{z_{arm}}.\overrightarrow{z_1} \neq 0$. This is equivalent to $\alpha_1 \neq \pm\frac{\pi}{2}$ and this is a singular value to be avoided. In the rest of the study it is further considered that $\overrightarrow{z_{arm}}.\overrightarrow{z_1} \neq 0$.

- For $i = 2$, (3a) writes $dim(T_{\mathbf{S}_1} + T_{\mathbf{R}_2} + T_{\mathbf{L}_2}) = 6$.

Consider $t \in T_{\mathbf{L}_1}$ and $t' \in T_{\mathbf{R}_1}$, one has:

$$\exists(\alpha_1, \alpha_2, \alpha_3, \alpha_4) \quad \text{such that} \quad t = \sum_{i=1}^{4} \alpha_i\ t_i \tag{19}$$
$$\exists(\alpha'_1, \alpha'_2, \alpha'_3,) \quad \text{such that} \quad t' = \alpha'_1\ t_5 + \alpha'_2\ t_6 + \alpha'_3\ t_3 \tag{20}$$

Using $\overrightarrow{z_{arm}}.\overrightarrow{z_1} \neq 0$, one easily gets:

$$t = t' \Leftrightarrow \alpha_1 = \alpha_2 = \alpha_4 = \alpha'_1 = \alpha'_2 = 0 \quad . \tag{21}$$

or:

$$t = t' \Leftrightarrow t = \alpha_3\ t_3 = \alpha'_3\ t_3 \quad . \tag{22}$$

In other words, at point P_1:

$$T_{\mathbf{S}_1} = T_{\mathbf{R}_1} \cap T_{\mathbf{L}_1} = span(\{t_3\}) = span(\{(z_1^{\mathrm{T}}\ 0_3^{\mathrm{T}})^{\mathrm{T}}\}) \quad . \tag{23}$$

Writing now twists at point P_2, one gets: $T_{\mathbf{S}_1} = span(\{t_7\})$, $T_{\mathbf{R}_2} = span(\{t_8\})$ and $T_{\mathbf{L}_2} = span(\{t_9\ t_{10}\ t_{11}\ t_{12}\})$, with:

$$t_7 = (z_1^{\mathrm{T}}\ l\sin\theta_1 x_1^{\mathrm{T}})^{\mathrm{T}} \quad , \quad t_8 = (x_2^{\mathrm{T}}\ -l_2\ y_2^{\mathrm{T}})^{\mathrm{T}} \quad , \quad t_9 = (x_2^{\mathrm{T}}\ 0^{\mathrm{T}})^{\mathrm{T}}$$
$$t_{10} = (y_2^{\mathrm{T}}\ 0^{\mathrm{T}})^{\mathrm{T}} \quad , \quad t_{11} = (z_2^{\mathrm{T}}\ 0^{\mathrm{T}})^{\mathrm{T}} \quad , \quad t_{12} = (0^{\mathrm{T}}\ z_{forearm}^{\mathrm{T}})^{\mathrm{T}},$$

where $\overrightarrow{P_1P_2} =: l\vec{z}$ and $\theta_1 := \left(\widehat{\overrightarrow{z_1}, \overrightarrow{z}}\right)$ measured around $\vec{x}_1$. Thus $T_{\mathbf{S}_1} + T_{\mathbf{R}_2} + T_{\mathbf{L}_2} = span(\{t_7, t_8, t_9, t_{10}, t_{11}, t_{12}\})$.

Suppose first that $\sin\theta_1 = 0$. Then, denoting $\overrightarrow{z_1} = z_{1x}.\overrightarrow{x_2} + z_{1y}.\overrightarrow{y_2} + z_{1z}.\overrightarrow{z_2}$, one gets:

$$t_7 = z_{1x}t_9 \ + \ z_{1y}t_{10} \ + \ z_{1z}t_{12} \tag{24}$$

In this particular case, $\{t_7\ ..\ t_{12}\}$ is not a basis, which identifies a second singular configuration, when M_1, P_1 and P_2 are aligned. In the rest of the study we will thus assume that this singular configuration is also avoided, that is: $\sin\theta_1 \neq 0$.

Defining

$$t'_7 \ = \ \frac{(t_7 - z_{1x}t_9 - z_{1y}t_{10} - z_{1z}t_{12})}{l\sin\theta_1} = (0^{\mathrm{T}}\ x_1^{\mathrm{T}})^{\mathrm{T}} \quad \text{,and}$$
$$t'_8 \ = \ \frac{(t_{10} - t_8)}{l_2} = (0^{\mathrm{T}}\ y_2^{\mathrm{T}})^{\mathrm{T}} \quad ,$$

we get $[t'_7\ t'_8\ t'_9\ ..\ t'_{12}] = B.[t_7\ t_8\ ..\ t_{12}]$ with $det(B) = \frac{-1}{l_2 \sin\theta_1} \neq 0$. Thus $\tau_3 = \{t_7\ ..\ t_{12}\}$ is a basis of $\mathbb{R}^6$ if and only if $\tau_4 = \{t'_7\ ..\ t'_{12}\}$ is a basis of $\mathbb{R}^6$. Consider $b_i \in \mathbb{R},\ i \in \{1,..,6\}$ such that:

$$b_1 t'_7 + b_2 t'_8 + b_3 t_9 + b_4 t_{10} + b_5 t_{11} + b_6 t_{12} = 0\ . \qquad (25)$$

It comes easily that $b_3 = b_4 = b_5 = 0$ and $b_1 t'_7 + b_2 t'_8 + b_6 t'_{12} = 0$ which is equivalent to $b_1 \overrightarrow{x_1} + b_2 \overrightarrow{y_2} + b_6 \overrightarrow{z_{forearm}} = \overrightarrow{0}$. The necessary and sufficient conditions to have a non-null triplet b_1, b_2, b_6 verifying the previous equation is that $\overrightarrow{x_1}, \overrightarrow{y_2}, \overrightarrow{z_{forearm}}$ are coplanar. This identifies a third singularity, which, again, is supposed to be avoided in the rest of the study.

2) Examination of the condition (3b)

- For $i = 1$, since $T_{\mathbf{S}_0} = \{0\}$, one directly gets $dim(T_{\mathbf{S}_0} \cap T_{\mathbf{L}_1}) = 0$.
- For $i = 2$, it is necessary to verify that $dim(T_{\mathbf{S}_1} \cap T_{\mathbf{L}_2}) = 0$.

Consider $t \in T_{\mathbf{S}_1}$ and $t' \in T_{\mathbf{L}_2}$. One has:

$$\begin{aligned} \exists \alpha_1 \in \mathbb{R} \quad / \quad & t = \alpha_1 t_7 \\ \exists \alpha'_1, \alpha'_2, \alpha'_3, \alpha'_4 \in \mathbb{R} \quad / \quad & t' = \alpha'_1 t_9 + \alpha'_2 t_{10} + \alpha'_3 t_{11} + \alpha'_4 t_{12}\ . \end{aligned}$$

One easily shows that $t = t'$ is equivalent to:

$$\begin{cases} \alpha_1 l \sin\theta_1 \overrightarrow{x_1} + \alpha'_4 \overrightarrow{z_{forearm}} = \overrightarrow{0} \\ (\alpha_1 z_{1x} + \alpha'_1)\overrightarrow{x_2} + (\alpha_1 z_{1y} + \alpha'_2)\overrightarrow{y_2} + (\alpha_1 z_{1z} + \alpha'_3)\overrightarrow{z_2} = \overrightarrow{0} \end{cases}$$

Since $\overrightarrow{x_1}$ is not colinear to $\overrightarrow{z_{forearm}}$, the first equation leads to $\alpha_1 = \alpha'_4 = 0$. Similarly, since $\{\overrightarrow{x_2}, \overrightarrow{y_2}, \overrightarrow{z_2}\}$ forms a basis, $\alpha'_1 = \alpha'_2 = \alpha'_3 = 0$. In conclusion, $dim(T_{\mathbf{S}_1} \cap T_{\mathbf{L}_2}) = \{0\}$.

3) Examination of the condition (3c)

For the considered example, $n = 2$ and condition (3c) writes $dim(T_{\mathbf{S}_2}) = 0$. Since $T_{\mathbf{S}_2} = (T_{\mathbf{S}_1} + T_{\mathbf{R}_2}) \cap T_{\mathbf{L}_2}$, we need to verify that any vector that belongs to both $(T_{\mathbf{S}_1} + T_{\mathbf{R}_2})$ and $T_{\mathbf{L}_2}$ is null. Consider $t \in (T_{\mathbf{S}_1} + T_{\mathbf{R}_2})$ and $t' \in T_{\mathbf{L}_2}$. One has:

$$\begin{aligned} \exists\ \alpha_1, \alpha_2 \in \mathbb{R} \quad / \quad & t = \alpha_1 t_7 + \alpha_2 t_8 \\ \exists\ \alpha'_1, .., \alpha'_4 \in \mathbb{R} \quad / \quad & t' = \alpha'_1 t_9 + \alpha'_2 t_1 0 + \alpha'_3 t_1 1 + \alpha'_4 t_1 2 \end{aligned}$$

Therefore $t = t'$ is equivalent to:

$$\begin{cases} \alpha_1 l \sin\theta_1 \overrightarrow{x_1} - \alpha_2 l_2 \overrightarrow{y_2} + \alpha'_4 \overrightarrow{z_{forearm}} = \overrightarrow{0} \\ (\alpha_1 z_{1x} + \alpha'_1 + \alpha_2)\overrightarrow{x_2} + (\alpha_1 z_{1y} + \alpha'_2)\overrightarrow{y_2} + (\alpha_1 z_{1z} + \alpha'_3)\overrightarrow{z_2} = \overrightarrow{0} \end{cases}$$

The first of these two equations leads to $\alpha_1 = \alpha_2 = \alpha'_4 = 0$ since it is supposed that $\overrightarrow{x_1}, \overrightarrow{y_2}$ and $\overrightarrow{z_{forearm}}$ are not coplanar in order to avoid the third singularity, and $\sin\theta_1 \neq 0$ in order to avoid the second singularity. Therefore, the second equation leads to $\alpha_1 = \alpha_2 = \alpha'_4 = 0$ because $\{\overrightarrow{x_2}, \overrightarrow{y_2}, \overrightarrow{z_2}\}$ forms a basis. In conclusion, $t = t' \Rightarrow t = 0$, or $dim(T_{\mathbf{S}_2}) = 0$.

4) Summary.

In conclusion, we identified three singularities:

1) $\overrightarrow{z_{arm}}.\overrightarrow{z_1} = 0$ representing the case where the passive slide, mounted parallel to the upper arm axis, is perpendicular to the robot upper limb axis. This case will never appear since the angle between $\overrightarrow{z_{arm}}$ and $\overrightarrow{z_1}$ reflects small discrepancies between the exoskeleton and human kinematics, and remains smaller than a few degrees.
2) $\sin\theta_1 = 0$ representing the case where M_1, P_1 and P_2 are aligned. This singular configuration can be avoided by limiting the range of motion for the robot elbow to a few degrees before full extension.
3) $\overrightarrow{x_1}, \overrightarrow{y_2}$ and $\overrightarrow{z_{forearm}}$ coplanar. This configuration does not appear in practice, since in the nominal configuration, $\overrightarrow{x_1}$ is perpendicular to the plane generated by $\overrightarrow{y_2}$ and $\overrightarrow{z_{forearm}}$.

Therefore, under normal conditions of operation, the ABLE exoskeleton with its two fixations never falls into a singular configuration.

REFERENCES

[1] A.B. Zoss, H. Kazerooni, and A. Chu. Biomechanical design of the berkeley lower extremity exoskeleton (bleex). *Mechatronics, IEEE/ASME Transactions on*, 11(2):128 –138, april 2006.

[2] M. Mihelj, T. Nef, and R. Riener. Armin ii - 7 dof rehabilitation robot: mechanics and kinematics. In *Robotics and Automation, 2007 IEEE International Conference on*, pages 4120 –4125, 10-14 2007.

[3] J.C. Perry, J. Rosen, and S. Burns. Upper-limb powered exoskeleton design. *Mechatronics, IEEE/ASME Transactions on*, 12(4):408 –417, aug. 2007.

[4] Jos L. Pons. *Wearable Robots: Biomechatronic Exoskeletons*. Wiley, April 2008.

[5] Stephen H. Scott and David A. Winter. Biomechanical model of the human foot: Kinematics and kinetics during the stance phase of walking. *Journal of Biomechanics*, 26(9):1091–1104, September 1993.

[6] F.C.T. Van der Helm, H.E.J. Veeger, G.M. Pronk, L.H.V. Van der Woude, and R.H. Rozendal. Geometry parameters for musculoskeletal modelling of the shoulder system. *Journal of Biomechanics*, 25(2):129–144, February 1992.

[7] A. Schiele. An explicit model to predict and interpret constraint force creation in phri with exoskeletons. In *Robotics and Automation, 2008. ICRA 2008. IEEE International Conference on*, pages 1324 –1330, 19-23 2008.

[8] A. Schiele and F.C.T. van der Helm. Kinematic design to improve ergonomics in human machine interaction. *Neural Systems and Rehabilitation Engineering, IEEE Transactions on*, 14(4):456 –469, dec. 2006.

[9] D. Cai, P. Bidaud, V. Hayward, and F. Gosselin. Design of self-adjusting orthoses for rehabilitation. In *Robotics and Applications, RA 2009 International Conference Robotics and Applications (RA 2009)*, November 2009.

[10] L W Lamoreux. Kinematic measurements in the study of human walking. *Bull Prosthet Res.*, 10(15):3–84, 1971. PMID: 5131748.

[11] KL Markolf, JS Mensch, and HC Amstutz. Stiffness and laxity of the knee–the contributions of the supporting structures. a quantitative in vitro study. *J Bone Joint Surg Am*, 58(5):583–594, 1976.

[12] C. Diez-Martnez, J. Rico, J. Cervantes-Snchez, and J. Gallardo. Mobility and connectivity in multiloop linkages. In *Advances in Robot Kinematics*, pages 455–464. 2006.

[13] K. J. Waldron. The constraint analysis of mechanisms. *Journal of Mechanisms*, 1(2):101–114, 1966.

[14] N. Jarrasse and G. Morel. A methodology to design kinematics of fixations between an orthosis and a human member. In *Advanced Intelligent Mechatronics, 2009 IEEE/ASME International Conference on*, Jul. 2009.

[15] P. Garrec, J.P. Friconneau, Y. Measson, and Y. Perrot. Able, an innovative transparent exoskeleton for the upper-limb. *Intelligent Robots and Systems, 2008. IROS 2008. IEEE/RSJ International Conference on*, pages 1483–1488, Sept. 2008.

[16] Garrec. P. French patent: Transmission vis, ecrou et cable attache a la vis - fr0101630, 2000 (eur 01938347.0-2421 and us 10/296,740 (screw and nut transmission and cable). 2000.